

# Detection and control of individual nuclear spins using a weakly coupled electron spin

T. H. Taminiau<sup>1</sup>, J. J. T. Wagenaar<sup>1</sup>, T. van der Sar<sup>1</sup>,  
F. Jelezko<sup>2</sup>, V. V. Dobrovitski<sup>3</sup>, and R. Hanson<sup>1</sup>

<sup>1</sup>*Kavli Institute of Nanoscience, Delft University of Technology,  
PO Box 5046, 2600 GA Delft, The Netherlands.*

<sup>2</sup>*Institut für Quantenoptik, Universität Ulm, 89081 Ulm, Germany.*

<sup>3</sup>*Ames Laboratory and Iowa State University, Ames, Iowa 50011, USA.*

(Dated: March 4, 2013)

We experimentally isolate, characterize and coherently control up to six individual nuclear spins that are weakly coupled to an electron spin in diamond. Our method employs multi-pulse sequences on the electron spin that resonantly amplify the interaction with a selected nuclear spin and at the same time dynamically suppress decoherence caused by the rest of the spin bath. We are able to address nuclear spins with interaction strengths that are an order of magnitude smaller than the electron spin dephasing rate. Our results provide a route towards tomography with single-nuclear-spin sensitivity and greatly extend the number of available quantum bits for quantum information processing in diamond.

Detecting the weak magnetic moment of a single nuclear spin presents the ultimate limit of sensitivity in magnetic resonance imaging [1–3]. Furthermore, nuclear spins may play a key role as qubits with long coherence times in quantum information technologies [4]. Addressing and controlling single nuclear spins is challenging because the spins are generally embedded in a noisy environment, such as a surrounding bath of nuclear spins.

The electron spin of a nitrogen-vacancy (NV) center is a powerful probe of its local magnetic environment [2, 3, 5–11]. If a single or a few nuclear spins are located particularly close to an NV center, the hyperfine interaction can well exceed the electron spin dephasing rate  $1/T_2^*$  [12]. Such strongly coupled nuclear spins are readily distinguished from the rest of the spin bath [13, 14] and can be selectively addressed and controlled [15–22]. However, typically the nuclear spin of interest is embedded in a bath of fluctuating nuclear spins. As a result, the coupling of this single nuclear spin to the NV center is weak compared to the rate of electron spin dephasing induced by the spin bath. For both magnetometry and quantum information purposes it would be greatly beneficial to be able to individually resolve and address such weakly coupled nuclear spins.

In this Letter, we isolate, characterize and selectively control up to six weakly coupled  $^{13}\text{C}$  nuclear spins that are embedded in the spin bath surrounding an NV center. The weak signal of a specific nuclear spin is amplified by precisely tuning a multi-pulse control sequence on the NV electron spin into resonance with the electron-nuclear spin dynamics [23]. At the same time this sequence dynamically decouples the electron spin from all other nuclear spins [24–26]. With this technique, we are able to resolve and coherently control nuclear spins with couplings that are an order of magnitude smaller than the dephasing rate of the NV center. Our results can enable tomography with single nuclear spin sensitivity and have the potential to greatly extend the number of solid-state

spin qubits available for quantum information processing.

Our method to isolate a weakly coupled nuclear spin from a background of other nuclear spins is based on the distinct conditional precession of each nuclear spin due to its particular hyperfine interaction with the NV electron spin ( $S = 1$ ), Fig. 1(a). For the electron in  $m_s = 0$ , all nuclear spins precess with the Larmor frequency

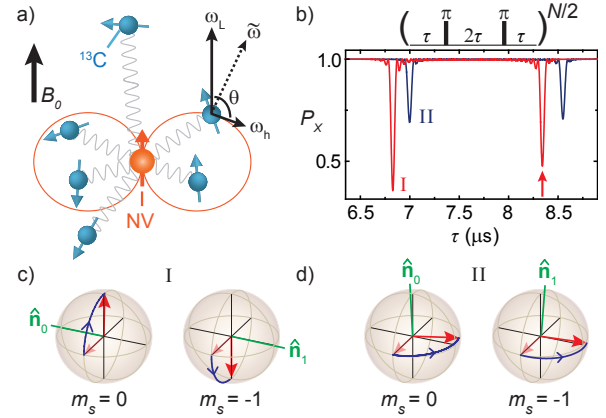


FIG. 1: Concept of isolating and controlling weakly coupled spins. (a) Surrounding  $^{13}\text{C}$  nuclear spins precess about axes that depend on the NV electron spin state. For  $m_s = 0$ , all  $^{13}\text{C}$  spins precess about  $\omega_L$  set by the applied magnetic field  $\mathbf{B}_0$ . For  $m_s = -1$ , each spin precesses about a distinct axis  $\hat{\omega}$  due to the hyperfine interaction  $\omega_h$ . (b) Calculated probability  $P_x$  to preserve the initial electron spin state after a decoupling sequence with  $N = 32$ , for two  $^{13}\text{C}$  spins with  $\theta = \pi/4.5$ , Nucleus I:  $\omega_h = 2\pi \cdot 40$  kHz, Nucleus II:  $\omega_h = 2\pi \cdot 20$  kHz,  $B_0 = 293$  G. Each spin can be selectively addressed by tuning the inter-pulse delay  $2\tau$  into resonance with its dynamics. (c,d) Bloch spheres showing the nuclear spin dynamics for  $\tau$  resonant with nucleus I (arrow). (c) For nucleus I, the net result is a rotation around anti-parallel axes ( $\hat{\mathbf{n}}_0$  and  $\hat{\mathbf{n}}_1$ ) for the two electron states, resulting in entanglement. (d) Nucleus II is decoupled: its rotation is independent of the electron state.

$\omega_L$  around an axis parallel to the applied magnetic field  $\mathbf{B}_0$ . For  $m_s = -1$ , each nuclear spin precesses around a distinct axis  $\tilde{\omega} = \omega_L + \omega_h$ . The hyperfine interaction  $\omega_h$  depends on the position of that particular nuclear spin relative to the NV center.

We can probe this conditional interaction by preparing the electron spin in a superposition,  $|x\rangle = (|m_s = 0\rangle + |m_s = -1\rangle)/\sqrt{2}$ , and applying a dynamical decoupling sequence consisting of  $N$  sequential  $\pi$ -pulses. Consider the basic decoupling unit on the electron spin  $\tau - \pi - 2\tau - \pi - \tau$ , in which  $\tau$  is a free evolution time (Fig. 1(b)). The net result of this unit is a rotation of the nuclear spin by an angle  $\phi$  around an axis  $\hat{\mathbf{n}}_i$  that depends on the initial state of the electron spin:  $\hat{\mathbf{n}}_0$  for initial state  $m_s = 0$  and  $\hat{\mathbf{n}}_1$  for initial state  $m_s = -1$  [23, 27].

If  $\hat{\mathbf{n}}_0$  and  $\hat{\mathbf{n}}_1$  are not parallel, the resulting conditional rotation of the nuclear spin generally entangles the electron and nuclear spins. As a result, for an unpolarized nuclear spin state, the final electron spin state is a statistical mixture of  $|x\rangle$  and  $|-x\rangle = (|m_s=0\rangle - |m_s=-1\rangle)/\sqrt{2}$ . The probability that the initial state  $|x\rangle$  is preserved is given by

$$P_x = (M + 1)/2, \quad (1)$$

with for a single nuclear spin:

$$M = 1 - (1 - \hat{\mathbf{n}}_0 \cdot \hat{\mathbf{n}}_1) \sin^2 \frac{N\phi}{2}. \quad (2)$$

For multiple nuclear spins that do not mutually interact,  $M$  is given by the product of all the individual values  $M_j$  for each individual spin  $j$ . Analytical expressions for  $\phi$  and for the angle between  $\hat{\mathbf{n}}_0$  and  $\hat{\mathbf{n}}_1$  as a function of the hyperfine interaction  $\omega_h$  and the inter-pulse delay  $\tau$  are given in the supplemental material [27].

As an example, Fig. 1(b) shows calculated results for two  $^{13}\text{C}$  spins with different hyperfine interactions. For most values of  $\tau$  the NV spin is effectively decoupled from both nuclear spins and its initial state is conserved ( $P_x \approx 1$ ). For specific values of  $\tau$ , the sequence is precisely resonant for one of the  $^{13}\text{C}$  spins and a sharp dip in the signal is observed. Figures 1(c, d) illustrate the evolution of the nuclear spins at the resonance condition for nuclear spin I. At this value of  $\tau$ , the net rotation axes  $\hat{\mathbf{n}}_0$  and  $\hat{\mathbf{n}}_1$  for nuclear spin I are approximately *anti*-parallel and the resulting conditional rotation entangles nuclear spin I with the electron spin ( $P_x \approx 1/2$ ). In contrast, at the same value of  $\tau$ ,  $\hat{\mathbf{n}}_0$  and  $\hat{\mathbf{n}}_1$  are nearly parallel for nuclear spin II and the resulting unconditional rotation leaves the electron spin unaffected. These resonances appear periodically as a function of  $\tau$ .

More insight into the periodicity and depth of the resonances can be gained by considering the case of large magnetic field,  $\omega_L \gg \omega_h$ . In this case the positions of the resonances are given by [27]:

$$\tau_k = \frac{(2k - 1)\pi}{2\omega_L + A}, \quad (3)$$

where  $k = 1, 2, 3, \dots$  is the order of the resonance, and  $A$  is the parallel component of the hyperfine interaction  $A = \omega_h \cos \theta$ . Equation 3 shows that the position is a linear function of  $k$ . The amplitude of the resonances is governed by the rotation angle  $\phi$ , which is of order  $B/\omega_L$ , with  $B = \omega_h \sin \theta$  the perpendicular component of the hyperfine coupling. Although  $\phi$  is small, the total angle is amplified by the large number of pulses  $N$ , enabling the detection with maximum contrast even of weakly coupled spins. In this way a single nuclear spin can be isolated from a bath of spins by a judicious choice of the inter-pulse delay  $2\tau$  and the number of pulses  $N$ .

We experimentally demonstrate our method using an NV center in a type IIa diamond with a natural abundance of  $^{13}\text{C}$  nuclear spins (1.1%). All experiments are performed at room temperature with an applied magnetic field along the NV symmetry axis. The NV electron spin is prepared in  $m_s = 0$  by illumination with a 532 nm laser and read out through its spin-dependent fluorescence. The experimental setup is described in detail in Ref. 23.

We choose an NV center that shows no nearby strongly coupled  $^{13}\text{C}$  spins in the electron spin resonance (ESR) spectrum and Ramsey measurements. The hyperfine coupling to the NV spin of all individual  $^{13}\text{C}$  spins is thus weak compared to  $1/T_2^*$ : all individual nuclear spins are hidden in the spin bath.

The experimental signal for a decoupling sequence with 32  $\pi$ -pulses is shown in Fig. 2(a). We observe sharp dips and broader collapses in an approximately exponentially decaying signal (see Fig. 2(b) for a magnification). The broader collapses correspond to the overlapping signals of multiple nuclear spins in the spin bath, whose product tends to yield  $P_x \approx 0.5$ . The sharp dips are signatures of the resonances of individual  $^{13}\text{C}$  spins. These appear primarily for large  $\tau$  because the separation between resonances of different spins increases with the resonance order  $k$  (see Eq. 3). We exploit the linear dependence in Eq. 3 to identify five distinct  $^{13}\text{C}$  spins (Fig. 2(c)). The resonances assigned to these spins are indicated in Fig. 2(b).

With a fit based on Eq. 2 we are able to determine both the magnitude  $\omega_h$  and the angle  $\theta$  of the hyperfine coupling from the experimentally observed resonances in Fig. 2(b) for each of the five spins. These fits take the overall signal decay due to relaxation to  $m_s = +1$  and dephasing of the electron state into account [27]. Although nuclear spin 6 can not be clearly resolved from the spin bath with a sequence of 32 pulses (Fig. 2(b)), we can further increase the sensitivity by applying more pulses. For  $N = 96$  the signal for spin 6 is well-isolated from the spin bath (Fig. 2(d)), enabling the characterization of the hyperfine interaction.

The obtained values for the hyperfine interaction strength  $\omega_h$  and angle  $\theta$  for the six nuclear spins are listed in Table 1. These values should be compared to the min-

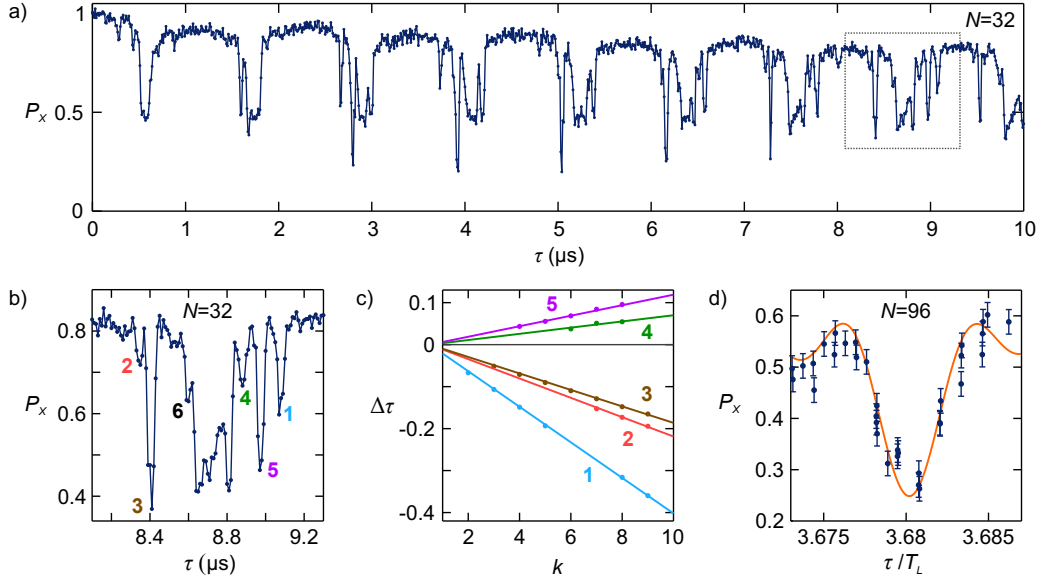


FIG. 2: Resolving individual weakly coupled  $^{13}\text{C}$  nuclear spins. (a)  $P_x$  as function of  $\tau$  for a decoupling sequence with  $N = 32$  and a magnetic field  $B_0 = 401$  G. The sharp resonances in the echo signal correspond to the coherent interaction with individual  $^{13}\text{C}$  atoms. (b) Magnification of the section marked in (a) indicating resonances associated with six nuclear spins. (c) Positions  $\tau_k$  of resonances with order  $k$  observed in (a) relative to the Larmor period  $T_L = 2\pi/\omega_L$ ,  $\Delta\tau = \tau_k/T_L - (2k - 1)/4$ . The five sets of equally-spaced resonances correspond to the spins numbered in (b). Lines are fits to Eq. 3. (d) Close up for nuclear spin 6 ( $\tau \approx 8.57 \dots 8.59 \mu\text{s}$ ) with  $N = 96$ . Line: fit based on equation 2. Errors are  $\pm 1$  standard deviation (s.d.).

Spin	$\omega_h/2\pi$ (kHz)	$\theta$ (degrees)
1	83.8(6)	21(1)
2	47(2)	30(5)
3	55(2)	54(2)
4	19(1)	133(3)
5	33(1)	132(1)
6	25.1(7)	51(2)

TABLE I: Hyperfine coupling strength  $\omega_h$  and angle  $\theta$  for the six nuclear spins identified in Fig. 2. These values were obtained by fitting a single well-isolated resonance for each nuclear spin based on Eq. 2. Uncertainties are 2 s.d.

imal coupling that can be resolved in an ESR measurement, which is given by the ESR line width. We find that our method detects hyperfine strengths as small as  $\sim 20$  kHz, about an order of magnitude smaller than the measured line width of  $\sqrt{2}/(\pi T_2^*) = 161(1)$  kHz. Furthermore, we resolve differences in hyperfine strength down to  $\sim 10$  kHz.

Assuming that the interaction is purely dipole-dipole, the values in Table 1 correspond to distances to the NV center between 0.6 and 1.2 nm. The fact that we can distinguish multiple weakly coupled spins beyond those that are coupled strongest to the NV demonstrates that our method can be used to create tomographic images of the spin environment at the single nuclear spin level.

We validate our approach by calculating the signal expected from the values in Table 1, and comparing the result with independent measurements over a broad range

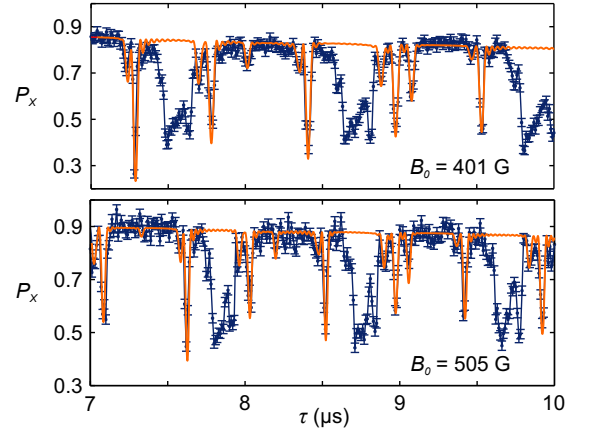


FIG. 3: Comparison of the measured signal with the prediction based on the parameters in Table 1 (orange line). We observe good agreement for the positions and amplitudes of multiple resonances for magnetic fields of both  $B_0 = 401$  G and  $B_0 = 505$  G. Error bars are  $\pm 1$  s.d.

of free evolution times at two different magnetic fields (Fig. 3). We find excellent agreement for both the positions and amplitudes of the resonances, confirming the accuracy of the theoretical model and the determined parameters.

Finally, we demonstrate that we can coherently rotate a weakly coupled nuclear spin over a desired angle by tuning the number of pulses  $N$ . Figure 4(a) plots the signal for a selected resonance ( $k = 8$ ) of spin 3 for dif-

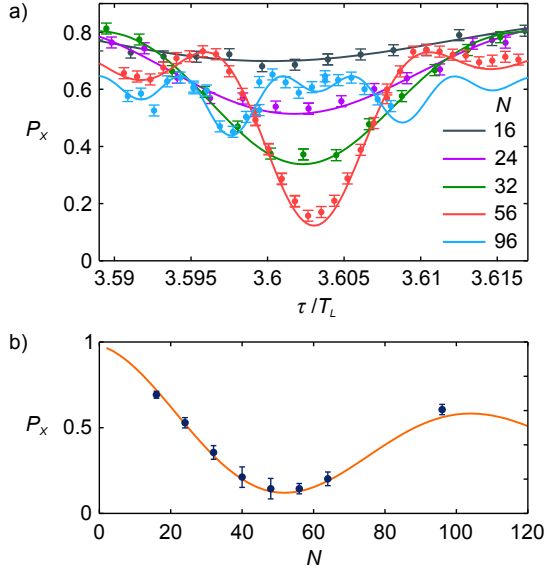


FIG. 4: Coherent conditional rotations of weakly-coupled nuclear spin 3. (a)  $P_x$  with different numbers of pulses  $N$  for the resonance centered at  $\tau \approx 8.4 \mu\text{s}$ . Lines: calculations based on the values in Table 1. Error bars:  $\pm 1$  s.d. (b)  $P_x$  at resonance as function of  $N$ . The experimental values are obtained from Gaussian fits. A fit using the values in Table 1 (line) yields a decay constant for the oscillation of  $1.8(3)$  ms (supplementary information). Uncertainties are 2 s.d.

ferent number of pulses  $N$ . The depth of the resonance first increases with  $N$  until the maximum contrast is obtained for  $N = \pi/\phi \approx 56$ . For more pulses the depth decreases again. In Fig. 4(b) we plot the signal at the center of the resonance as a function of  $N$ .

The oscillation observed in Fig. 4(b) demonstrates the coherent conditional rotation of a single weakly coupled  $^{13}\text{C}$  spin. For  $N = 28$  the signal reaches  $\sim 0.5$ . Here, the nuclear spin has rotated over an angle  $N\phi/2 \approx \pi/2$ , in a direction which is conditioned by the electron spin state (similar to the case illustrated in Fig. 1(c)). This sequence corresponds to a maximally entangling operation, equivalent to the quantum controlled-NOT gate up to single-qubit rotations. For  $N = 56$ , the nuclear spin has rotated over an angle  $N\phi/2 \approx \pi$ . Here, the two conditional rotations lead to the same final nuclear spin state up to a  $2\pi$  phase difference. This phase difference transfers to the electron spin, yielding the pure state  $|-x\rangle$  and signal  $P_x \approx 0$ .

Unconditional rotations of the nuclear spin can be implemented by using different values for  $\tau$  (see e.g. Fig. 1(d)) [23]. A combination of conditional and unconditional operations can be used to initialize the nuclear spin by swapping its state with the electron [15] or for reading out the nuclear spin state in a single-shot by mapping it onto the electron spin [18, 21, 22]. Our results thus indicate the possibility of using weakly coupled nuclear spins as fully controllable qubits.

The oscillation in Fig. 4(b) is damped on a timescale of a few ms. This timescale is consistent with the longitudinal relaxation of the electron spin at room temperature ( $T_1$  process) [28]. At cryogenic temperatures this relaxation time exceeds seconds [28], allowing for the implementation of high-precision quantum gates on weakly coupled  $^{13}\text{C}$  nuclei.

In conclusion, we have isolated, characterized and coherently controlled individual weakly coupled nuclear spins embedded in a spin bath. Because we address spins beyond the few nearest to the NV center, our method can enable the tomography of ensembles of spins in diamond and, potentially, in external samples [29]. In addition, the method enables coherent gates between the electron spin and weakly-coupled nuclear spins. Our results thus indicate a clear pathway for using weakly coupled nuclear spins as qubits, thereby eliminating the need for strong coupling and greatly extending the possible number of qubits within a local register.

*Author's note* - While finalizing this manuscript we became aware of two complementary studies that consider the sensing of weakly-coupled nuclear spins in the low magnetic field regime [30] and in isotopically purified diamond [31].

*Acknowledgements* - We thank S. Kolkowitz, M. D. Lukin, G. de Lange, H. Fedder and J. Wrachtrup for discussions. This work is supported by the Dutch Organization for Fundamental Research on Matter (FOM), the Netherlands Organization for Scientific Research (NWO), the DARPA QuEST program and the EU STREP program DIAMANT. THT acknowledges support by a Marie Curie Intra European Fellowship.

- 
- [1] C. L. Degen *et al.*, Proc. Nat. Acad. Sci. **106**, 1313 (2009).
  - [2] J. M. Taylor *et al.*, Nature Phys. **4**, 810 (2008).
  - [3] C. L. Degen, Appl. Phys. Lett. **92**, 243111 (2008).
  - [4] T. D. Ladd *et al.*, Nature **464**, 45 (2010).
  - [5] J. R. Maze *et al.*, Nature **455**, 644 (2008).
  - [6] G. Balasubramanian *et al.*, Nature **455**, 648 (2008).
  - [7] G. de Lange *et al.*, Phys. Rev. Lett. **106**, 080802 (2011).
  - [8] N. Zhao *et al.*, Nature Nanotech. **6**, 242 (2011).
  - [9] L. Rondin *et al.*, Appl. Phys. Lett. **100**, 153118 (2012).
  - [10] S. Kolkowitz *et al.*, Science **335**, 1603 (2012).
  - [11] L. T. Hall *et al.*, Phys. Rev. B **82**, 045208 (2010).
  - [12] L. Childress *et al.*, Science **314**, 281 (2006).
  - [13] B. Smeltzer *et al.*, New J. Phys. **13**, 025021(2011).
  - [14] A. Dr  au *et al.*, Phys. Rev. B **85**, 134107 (2012).
  - [15] M. V. G. Dutt *et al.*, Science **316**, 1312 (2007).
  - [16] P. Neumann *et al.*, Science **320**, 1326 (2008).
  - [17] B. Smeltzer *et al.*, Phys. Rev. A **80**, 050302 (2009).
  - [18] P. Neumann *et al.*, Science **329**, 542 (2010).
  - [19] M. Steiner *et al.*, Phys. Rev. B **81**, 035205 (2010).
  - [20] G. D. Fuchs *et al.*, Nature Phys. **7**, 789 (2011).
  - [21] L. Jiang *et al.*, Science **326**, 267 (2009).
  - [22] L. Robledo *et al.*, Nature **477**, 574 (2011).

- [23] T. van der Sar *et al.*, Nature **484**, 82 (2012).
- [24] G. de Lange *et al.*, Science **330**, 60 (2010).
- [25] C. A. Ryan *et al.*, Phys. Rev. Lett. **105**, 200402 (2010).
- [26] B. Naydenov *et al.*, Phys. Rev. B **83**, 081201 (2011).
- [27] See Supplemental Material for derivations of the equations used and a description of the fitting including relaxation and dephasing.
- [28] A. Jarmola *et al.*, arXiv:1112.5936v2 (2012).
- [29] J. -M. Cai *et al.*, arXiv:1112.5502v1 (2011).
- [30] S. Kolkowitz *et al.*, arXiv:1204.5483v1 (2012).
- [31] N. Zhao *et al.*, arXiv:1204.6513v1 (2012).

## SUPPLEMENTAL MATERIAL

### SYSTEM DYNAMICS DURING THE DECOUPLING SEQUENCE

In this section we derive the equations used in the main text. We consider the conditional dynamics of a nuclear spin that interacts with the NV electron spin through the hyperfine coupling.

#### Hamiltonian of the system

With an appropriate rotation of the coordinate axes, the Hamiltonian of the NV spin coupled to a single  $^{13}\text{C}$  spin is given by

$$\hat{H} = A\hat{S}_z\hat{I}_z + B\hat{S}_z\hat{I}_x + \omega_L\hat{I}_z = |0\rangle\langle 0|\hat{H}_0 + |1\rangle\langle 1|\hat{H}_1, \quad (4)$$

where  $\hat{S}_i$  ( $\hat{I}_i$ ) are the Pauli matrices of the electron (nuclear) spin,  $\omega_L$  is the nuclear Larmor frequency, and  $A = \omega_h \cos \theta$  ( $B = \omega_h \sin \theta$ ) is the parallel (perpendicular) component of the hyperfine coupling (see Fig. 1(a)). The nuclear spin evolves according to a Hamiltonian which is conditioned by the electron spin state:  $\hat{H}_0$  if the electron is in  $m_s = 0$  (state  $|0\rangle$ ), and  $\hat{H}_1$  if the electron is in  $m_s = -1$  (state  $|1\rangle$ ), with

$$\hat{H}_0 = \omega_L\hat{I}_z, \quad \text{and} \quad \hat{H}_1 = (A + \omega_L)\hat{I}_z + B\hat{I}_x. \quad (5)$$

#### Net result of the decoupling sequence

As described in the main text, we probe the conditional interaction by preparing the electron spin in  $|x\rangle = (|0\rangle + |1\rangle)/\sqrt{2}$ , driving it by a decoupling sequence with  $N/2$  decoupling units of the form  $\tau - \pi - 2\tau - \pi - \tau$  (Fig. 1(b)), and measuring the  $x$ -component of the NV electron spin at the end of the sequence.

The probability that the initial state  $|x\rangle$  is preserved is given by  $P_x = (M + 1)/2$ , with

$$M = \text{Re Tr}(\hat{U}_0\hat{U}_1^\dagger), \quad (6)$$

where  $U_0$  and  $U_1$  are the conditional evolution operators for the nuclear spin corresponding to the initial states of the NV spin  $m_s = 0$  and  $m_s = -1$  respectively. These operators, describing the evolution after  $N/2$  decoupling units, have the form  $U_0 = \hat{V}_0^{N/2}$  and  $U_1 = \hat{V}_1^{N/2}$ , where  $\hat{V}_0$  and  $\hat{V}_1$  are the conditional evolution operators for a single decoupling unit ( $N = 2$ ):

$$\hat{V}_0 = \exp[-i\hat{H}_0\tau] \exp[-i\hat{H}_12\tau] \exp[-i\hat{H}_0\tau] \quad (7)$$

$$\hat{V}_1 = \exp[-i\hat{H}_1\tau] \exp[-i\hat{H}_02\tau] \exp[-i\hat{H}_1\tau]. \quad (8)$$

Since any unitary evolution of a single qubit is a rotation, the conditional operators  $\hat{V}_0$  and  $\hat{V}_1$  can be represented

as

$$\hat{V}_0 = \exp[-i\phi(\hat{\mathbf{I}} \cdot \hat{\mathbf{n}}_0)] \quad (9)$$

$$\hat{V}_1 = \exp[-i\phi(\hat{\mathbf{I}} \cdot \hat{\mathbf{n}}_1)], \quad (10)$$

which illustrates that the net evolution of the nuclear spin after a single decoupling unit is a rotation by an angle  $\phi$  around an axis  $\hat{\mathbf{n}}_i$  that depends on the initial state of the electron spin:  $\hat{\mathbf{n}}_0$  for initial state  $m_s = 0$  and  $\hat{\mathbf{n}}_1$  for initial state  $m_s = -1$ . Note that the rotation angle  $\phi$  is independent of the electron spin input state because  $\cos \phi = \text{Tr} \hat{V}_0 = \text{Tr} \hat{V}_1$ .

With these expressions, we obtain Eq. 2 of the main text:

$$M = 1 - (1 - \hat{\mathbf{n}}_0 \cdot \hat{\mathbf{n}}_1) \sin^2 \frac{N\phi}{2}. \quad (11)$$

Thus, we only need to determine the net rotation angle  $\phi$  and the inner product  $\hat{\mathbf{n}}_0 \cdot \hat{\mathbf{n}}_1$  to completely characterize the signal.

#### Nuclear spin rotation axes and angle

Using eqs. 7- 10, we obtain expressions for the rotation angle  $\phi$  and the inner product  $\hat{\mathbf{n}}_0 \cdot \hat{\mathbf{n}}_1$ :

$$\cos \phi = \cos \alpha \cos \beta - m_z \sin \alpha \sin \beta \quad (12)$$

$$1 - \hat{\mathbf{n}}_0 \cdot \hat{\mathbf{n}}_1 = m_x^2 \frac{(1 - \cos \alpha)(1 - \cos \beta)}{1 + \cos \alpha \cos \beta - m_z \sin \alpha \sin \beta} \quad (13)$$

where  $m_z = (A + \omega_L)/\tilde{\omega}$ ,  $m_x = B/\tilde{\omega}$ , and  $\tilde{\omega} = \sqrt{(A + \omega_L)^2 + B^2}$ . For simplicity, we introduced the angles  $\alpha = \tilde{\omega}\tau$  and  $\beta = \omega_L\tau$ .

#### High magnetic field: $\omega_L \gg \omega_h$

The advantage of performing the experiments at high magnetic field, so that  $\omega_L \gg \omega_h$ , is that the signal  $M$  has a clear form: for most values of  $\tau$ , the depth of the signal modulation  $(1 - \hat{\mathbf{n}}_0 \cdot \hat{\mathbf{n}}_1)$  is small, of order of  $m_x^2 \sim B^2/\omega_L^2$ . Here, the axes  $\hat{\mathbf{n}}_0$  and  $\hat{\mathbf{n}}_1$  are practically parallel and the nuclear spin undergoes an unconditional rotation (Fig 1(d)). The modulation is only strong when the decoupling sequence is precisely resonant with the nuclear spin dynamics. At resonance, the axes  $\hat{\mathbf{n}}_0$  and  $\hat{\mathbf{n}}_1$  are antiparallel, i.e.  $\hat{\mathbf{n}}_0 \cdot \hat{\mathbf{n}}_1 = -1$ , leading to a conditional rotation of the nuclear spin (Fig. 1(c)). The condition for the resonances is

$$\tan \frac{\alpha}{2} \tan \frac{\beta}{2} = \frac{1}{m_z}. \quad (14)$$

For the high magnetic field case where  $m_x \ll 1$ , in first order in this small quantity, the solution for Eq. 14 is  $\alpha = -(\beta + \pi) + 2k\pi$  with any integer  $k$ , so that

$\tan(\alpha/2) = 1/\tan(\beta/2)$ , and the corrections are of the second order in  $m_x$ . In this case the inter-pulse distance  $2\tau$  corresponding to the resonance condition satisfies

$$\tau = \tau_k \approx \frac{(2k+1)\pi}{2\omega_L + A}, \quad (15)$$

which is equivalent to the Eq. 3 of the main text.

We now provide more insight into the shape and amplitude of the resonances. To understand what happens when  $\tau$  is varied from the resonant value  $\tau_k$ , we assume that  $\tau = \tau_k(1+\Delta)$  with small  $\Delta$ . Then, the inner product of the rotation axes becomes

$$1 - (\hat{\mathbf{n}}_0 \cdot \hat{\mathbf{n}}_1) = 2/(1 + \delta_k^2/m_x^2), \quad (16)$$

where  $\delta_k = (2k+1)\pi\Delta$ , and we assume as above that  $A, B \ll \omega_L$ . Thus, this modulation depth as a function of  $\Delta$  is a Lorentzian with a small width of  $m_x/[(2k+1)\pi]$  (this justifies our assumption about  $\Delta$  being small, not exceeding  $m_x \ll 1$  too much). The final result as a function of  $\delta_k$  acquires the form

$$M = 1 - \frac{2}{1 + \delta_k^2/m_x^2} \sin^2 \left[ \frac{N}{2} \sqrt{m_x^2 + \delta_k^2} \right]. \quad (17)$$

This expression demonstrates that even when  $m_x \ll 1$  the resonance can be visible. When the argument of the sine function above is small, the amplitude of the resonance is of order  $m_x^2 N^2$ , and is therefore amplified by a factor of  $N^2$ . By increasing the number of pulses, we increase the sensitivity of the detection of the nuclear spins, i.e. we can address more and more nuclei, which are coupled weaker and weaker to the NV spin.

## ELECTRON SPIN RELAXATION AND DEPHASING

For the fits in the main text we take the overall decay of the signal due to the relaxation and dephasing of the electron spin into account. The equation relating the obtained signal  $P_x$  to the modulation  $M$  due to the interaction with the nuclear spins becomes:

$$P_x = 1/2 e^{-2N\tau/T_\alpha} M + 1/3 + 1/6 e^{-2N\tau/T_\beta}, \quad (18)$$

in which  $T_\alpha$  and  $T_\beta$  are two phenomenological time constants. Note that at  $\tau = 0$  the signal modulation is maximum and equation 18 is equivalent to the ideal case given in the text.

$T_\beta$  describes the  $T_1$  relaxation of the electron spin into the  $m_s = +1$  sublevel. This relaxation affects the center value that the modulation  $M$  acts on. We measure this time constant by taking the average value of the outcomes of measurements along  $x$  and  $-x$  ( $|-x\rangle = (|0\rangle - |1\rangle)/\sqrt{2}$ ), i.e. effectively we measure for  $M = 0$ . We obtain  $T_\beta = 2.2$  ms.

$T_\alpha$  accounts for dephasing of the electron spin and includes not-decoupled dephasing, microwave pulse errors and decoherence due to  $T_1$  relaxation. These effects reduce the total modulation amplitude. This reduction is only approximately exponential, but this is a good approximation over the small  $\tau$  ranges that are used for the fits. The values obtained from fits vary between 1.3 and 2.2 ms for different measurements depending on the number of pulses, the fidelity of the  $\pi$ -pulses, and the applied magnetic field.